NUMERICAL SOLUTION OF THE INVISCID STAGNATION-FLOW SOLIDIFICATION PROBLEM

R. H. Rangel[1] and X. Bian

Department of Mechanical and Aerospace Engineering
University of California, Irvine
Irvine, CA 92717 USA

Phone : (714) 824-4033
Fax : (714) 824-8585

email : rhrangel@uci.edu

Abstract

The inviscid stagnation-flow solidification problem is investigated by applying the finite-difference method after a coordinate transformation to a fixed domain. Numerical solutions of the temperature distribution, the solid-liquid interface location as well as its growth rate are obtained, and comparisons with the instantaneous-similarity solution and the quasi-steady solution are made. Since the transformed system of equations for this solidification problem has a singularity at $t = 0$, the finite-difference solution is started at a small time using the instantaneous-similarity solution as the initial field. The numerical solution confirms the existence of an asymptotic limit of the solidification front as previously demonstrated by means of both a quasi-steady and an instantaneous-similarity solution.

Published in

Numerical Heat Transfer, Part A: Applications, 28, No.5, 589-603, 1995

[1] Author to whom correspondence should be addressed.

Nomenclature

A	potential-flow strain rate
B	variable defined as $\tilde{s}^2$
a	ratio of the liquid to solid thermal diffusivity (α_ℓ/α_s)
b	ratio of the liquid to solid thermal conductivity (k_ℓ/k_s)
c_p	specific heat
h_{sf}	latent heat of solidification
i	grid point in x' direction
I	total grid points in x' direction
k	thermal conductivity
L_c	characteristic length ($\sqrt{\alpha_s/A}$)
q''	heat flux
s	solid phase thickness
S_t	Stefan number
T	temperature
t	time
u	velocity component of liquid phase in x direction
v	velocity component of liquid phase in y direction
x	spatial coordinate normal to the substrate
x'	transformed coordinate $[2/\pi \tan^{-1}(x/s)]$
y	spatial coordinate parallel to the substrate

Greek symbols

α	thermal diffusivity
ρ	density
θ	nondimensional temperature $[(T - T_m)/(T_m - T_0)]$
τ	nondimensional time (At)

Subscripts

i	initial
ℓ	liquid phase
o	substrate
m	melting
p	iteration index
s	solid phase

Superscripts

$\sim$	nondimensional
n	discrete-time index

1. Introduction

Heat transfer accompanied by liquid-solid phase change is of great importance in many industrial applications such as casting, welding and spray forming. The physical phenomena associated with the behavior of the solid-liquid interface and the heat transfer in both the solid and liquid phases have been the subject of several numerical and analytical studies [1]-[12].

Examples of analytical or semi-analytical solutions to phase change problems are those of Cho and Sunderland [1] and Madejski [2][3]. The most classical exact solution is probably the so called Neumann solution of the Stefan problem [13]-[15] which predicts the temperature distribution and rate of solidification (or melting) of a semi-infinite medium.

With the development of high-speed computers, numerical methods have been developed as tools for the study of phase-change processes. Most of them are summarized in [16]. The numerical methods used can be divided into two groups [5]: the enthalpy method and the interface-tracking method. In the first group, enthalpy and temperature are dependent variables for the energy equation. The location of the phase change interface is determined from the calculated enthalpy. In the second group, the temperature and the solid-liquid interface location are the dependent variables and the energy conservation equations are written separately for the solid and the liquid regions. The major difficulty with this technique arises from the need to track a continuously moving phase interface. The rate of propagation of this boundary into the liquid region (solidification) or into the solid region (melting) depends on the thermal properties of the solid and liquid phases, and in addition, in the cases where there exists motion in the liquid phase, such as metal droplet deposition, it also depends on the fluid properties of the liquid region. Various procedures have been developed to deal with this problem [6] [7], but most of them have addressed the cases in which there is no liquid motion, or they simply have taken into account heat conduction as the sole heat transfer mechanism [8] [9]. A notable exception is reported in [10] where a boundary-conforming adaptive coordinate system is used to track the interface. Those investigations on the droplet deformation and solidification behavior during impingement on a cold substrate in the spray processing mainly

rely on the classical Neumann solution of the Stefan solidification model to determine the solid-liquid interface position [2], [11], [12]. The major shortcoming of these procedures is that the classical Stefan model corresponds to a stagnant liquid phase. An appropriate heat transfer and solidification model should account for convective effects due to fluid motion.

Recently, a heat transfer and solidification model for the inviscid two-dimensional stagnation flow was developed by Rangel and Bian [17] to investigate the effect of the liquid motion on its solidification behavior in the process of the moving liquid impinging on a cold substrate. A stability study of the stagnation-flow problem was presented in [4]. In the present work, a finite-difference solution of the stagnation-flow solidification problem is obtained and compared with the semi-analytical solution. The results provide insight into situations such as the deformation and solidification of a droplet impinging on a cold substrate in the spray forming process.

2. Numerical solution

The set of governing equations for the inviscid stagnation-flow solidification problem is [17]:

$$\frac{\partial \theta_s}{\partial t} = \alpha_s \frac{\partial^2 \theta_s}{\partial x^2} \qquad \text{for} \quad 0 < x < s(t) \tag{1}$$

$$\frac{\partial \theta_\ell}{\partial t} - 2A(x - s(t))\frac{\partial \theta_\ell}{\partial x} = \alpha_\ell \frac{\partial^2 \theta_\ell}{\partial x^2} \qquad \text{for} \quad s(t) < x < \infty \tag{2}$$

$$\theta_\ell = \theta_s \qquad \text{and} \quad k_s \frac{\partial \theta_s}{\partial x} - k_\ell \frac{\partial \theta_\ell}{\partial x} = \frac{k_s}{\alpha_s}\frac{1}{S_t}\frac{ds}{dt} \qquad \text{at} \quad x = s(t) \tag{3}$$

New variables (x', τ) are introduced and the coordinates (x, t) are transformed to (x', τ), where

$$x' = \frac{2}{\pi}\tan^{-1}(\frac{x}{s}) \tag{4}$$

$$\tau = At \tag{5}$$

The spatial transformation serves two purposes: it transforms the semi-infinite domain into a finite one, and it converts the moving-interface problem into a fixed-interface problem. A similar transformation was employed by Campo and Auguste [18] in a problem of heat transfer in a pipe.

The metrics of the transformation are:

$$\frac{\partial \tau}{\partial t} = A \tag{6}$$

$$\frac{\partial \tau}{\partial x} = 0 \tag{7}$$

$$\frac{\partial x'}{\partial t} = -\frac{A}{\pi}\sin(\pi x')\frac{1}{s}\frac{ds}{d\tau} \tag{8}$$

$$\frac{\partial x'}{\partial x} = \frac{2}{\pi}\cos^2(\frac{\pi}{2}x')\frac{1}{s} \tag{9}$$

$$\frac{\partial^2 x'}{\partial x^2} = -\frac{2}{\pi}\sin(\pi x')\cos^2(\frac{\pi}{2}x')\frac{1}{s^2} \tag{10}$$

so that:

$$\frac{\partial}{\partial t} = -\frac{A}{\pi}\sin(\pi x')\frac{1}{s}\frac{ds}{d\tau}\frac{\partial}{\partial x'} + A\frac{\partial}{\partial \tau} \tag{11}$$

$$\frac{\partial}{\partial x} = \frac{2}{\pi}\cos^2(\frac{\pi}{2}x')\frac{1}{s}\frac{\partial}{\partial x'} \tag{12}$$

$$\frac{\partial^2}{\partial x^2} = -\frac{2}{\pi}\sin(\pi x')\cos^2(\frac{\pi}{2}x')\frac{1}{s^2}\frac{\partial}{\partial x'} + \frac{4}{\pi^2}\cos^4(\frac{\pi}{2}x')\frac{1}{s^2}\frac{\partial^2}{\partial x'^2} \tag{13}$$

Introducing the nondimensional variable

$$\tilde{s} = s/L_c \tag{14}$$

where $L_c = \sqrt{\alpha_s/A}$ is a characteristic length. Eqs. (1)-(3) are transformed to

$$\begin{aligned}\frac{\partial \theta_s}{\partial \tau} &= \frac{4}{\pi^2}\cos^4(\frac{\pi}{2}x')\frac{1}{\tilde{s}^2}\frac{\partial^2\theta_s}{\partial x'^2} + \left[\frac{1}{\pi}\sin(\pi x')\frac{1}{\tilde{s}}\frac{d\tilde{s}}{d\tau}\right. \\ &\quad \left. -\frac{2}{\pi}\sin(\pi x')\cos^2(\frac{\pi}{2}x')\frac{1}{\tilde{s}^2}\right]\frac{\partial \theta_s}{\partial x'} \qquad \text{for} \quad 0 < x' < 0.5\end{aligned} \tag{15}$$

$$\begin{aligned}\frac{\partial \theta_\ell}{\partial \tau} &= \frac{4a}{\pi^2}\cos^4(\frac{\pi}{2}x')\frac{1}{\tilde{s}^2}\frac{\partial^2\theta_\ell}{\partial x'^2} + \left[\frac{1}{\pi}\sin(\pi x')\frac{1}{\tilde{s}}\frac{d\tilde{s}}{d\tau} - \frac{2a}{\pi}\sin(\pi x')\cos^2(\frac{\pi}{2}x')\frac{1}{\tilde{s}^2}\right. \\ &\quad \left. +\frac{2}{\pi}\sin(\pi x') - \frac{4}{\pi}\cos^2(\frac{\pi}{2}x')\right]\frac{\partial \theta_\ell}{\partial x'} \qquad \text{for} \quad 0.5 < x' < 1\end{aligned} \tag{16}$$

$$\theta_\ell = \theta_s \qquad \text{and} \quad \frac{\partial \theta_s}{\partial x'} - b\frac{\partial \theta_\ell}{\partial x'} = \frac{\pi}{S_t}\tilde{s}\frac{d\tilde{s}}{d\tau} \qquad \text{at} \quad x' = 0.5 \tag{17}$$

By applying the Crank-Nicolson method, Eqs. (15)-(16) can be written in finite-

difference form:

<u>Solid phase</u>:

$$\begin{aligned}\frac{\theta_s(n+1,i)-\theta_s(n,i)}{\Delta\tau} &= \frac{1}{2}\frac{4}{\pi^2}\cos^4(\frac{\pi}{2}x')\frac{1}{\tilde{s}^2}\left[\frac{\theta_s(n+1,i+1)-2\theta_s(n+1,i)+\theta_s(n+1,i-1)}{\Delta x'^2}\right.\\ &\left.+\frac{\theta_s(n,i+1)-2\theta_s(n,i)+\theta_s(n,i-1)}{\Delta x'^2}\right]\\ &+\frac{1}{2}\left[\frac{1}{\pi}\sin(\pi x')\frac{1}{\tilde{s}}\frac{d\tilde{s}}{d\tau}-\frac{2}{\pi}\sin(\pi x')\cos^2(\frac{\pi}{2}x')\frac{1}{\tilde{s}^2}\right]\\ &\left[\frac{\theta_s(n+1,i+1)-\theta_s(n+1,i-1)}{2\Delta x'}+\right.\\ &\left.\frac{\theta_s(n,i+1)-\theta_s(n,i-1)}{2\Delta x'}\right] \qquad \text{for } i=1,...I_s, \end{aligned} \tag{18}$$

with boundary conditions:

$\theta_s=-1$, at $x'=0$ $(i=0)$.

$\theta_s=0$, at $x'=0.5$ $(i=I_s+1)$.

<u>Liquid phase</u>:

$$\begin{aligned}\frac{\theta_\ell(n+1,i)-\theta_\ell(n,i)}{\Delta\tau} &= \frac{1}{2}\frac{4a}{\pi^2}\cos^4(\frac{\pi}{2}x')\frac{1}{\tilde{s}^2}\left[\frac{\theta_\ell(n+1,i+1)-2\theta_\ell(n+1,i)+\theta_\ell(n+1,i-1)}{\Delta x'^2}\right.\\ &\left.+\frac{\theta_\ell(n,i+1)-2\theta_\ell(n,i)+\theta_\ell(n,i-1)}{\Delta x'^2}\right]\\ &+\frac{1}{2}\left[\frac{1}{\pi}\sin(\pi x')\frac{1}{\tilde{s}}\frac{d\tilde{s}}{d\tau}-\frac{2a}{\pi}\sin(\pi x')\cos^2(\frac{\pi}{2}x')\frac{1}{\tilde{s}^2}+\frac{2}{\pi}\sin(\pi x')\right.\\ &\left.-\frac{4}{\pi}\cos^2(\frac{\pi}{2}x')\right]\left[\frac{\theta_\ell(n+1,i+1)-\theta_\ell(n+1,i-1)}{2\Delta x'}+\right.\\ &\left.\frac{\theta_\ell(n,i+1)-\theta_\ell(n,i-1)}{2\Delta x'}\right] \qquad \text{for } i=1,...I_\ell \end{aligned} \tag{19}$$

with boundary conditions:

$\theta_\ell=0$, at $x'=0.5$ $(i=0)$.

$\theta_\ell=\theta_i$, at $x'=1$ $(i=I_\ell+1)$.

Eq. (18) can be rewritten as

$$\begin{aligned}(1+2c_1)\theta_s(n+1,i) &= (c_1+c_2)\theta_s(n+1,i+1)+(c_1-c_2)\theta_s(n+1,i-1)+\\ &c_1[\theta_s(n,i+1)-2\theta_s(n,i)+\theta_s(n,i-1)]+\\ &c_2[\theta_s(n,i+1)-\theta_s(n,i-1)]+\theta_s(n,i) \end{aligned} \tag{20}$$

where

$$c_1 = \frac{2}{\pi^2}\cos^4(\frac{\pi}{2}x')\frac{1}{(\tilde{s}^2)^{n+1}}\frac{\Delta\tau}{\Delta x'^2} \tag{21}$$

$$c_2 = \left[\frac{1}{8\pi}\sin(\pi x')\frac{1}{(\tilde{s}^2)^{n+1}}\left(\frac{d\tilde{s}^2}{d\tau}\right)^{n+1} - \frac{1}{2\pi}\sin(\pi x')\cos^2(\frac{\pi}{2}x')\frac{1}{(\tilde{s}^2)^{n+1}}\right]\frac{\Delta\tau}{\Delta x'} \tag{22}$$

while Eq. (19) can be rewritten as

$$\begin{aligned}(1+2d_1)\theta_\ell(n+1,i) &= (d_1+d_2)\theta_\ell(n+1,i+1)+(d_1-d_2)\theta_\ell(n+1,i-1)+\\ &\quad d_1[\theta_\ell(n,i+1)-2\theta_\ell(n,i)+\theta_\ell(n,i-1)]+\\ &\quad d_2[\theta_\ell(n,i+1)-\theta_\ell(n,i-1)]+\theta_\ell(n,i)\end{aligned} \tag{23}$$

where

$$d_1 = \frac{2a}{\pi^2}\cos^4(\frac{\pi}{2}x')\frac{1}{(\tilde{s}^2)^{n+1}}\frac{\Delta\tau}{\Delta x'^2} \tag{24}$$

$$\begin{aligned}d_2 &= \left[\frac{1}{8\pi}\sin(\pi x')\frac{1}{(\tilde{s}^2)^{n+1}}\left(\frac{d\tilde{s}^2}{d\tau}\right)^{n+1} - \frac{a}{2\pi}\sin(\pi x')\cos^2(\frac{\pi}{2}x')\frac{1}{(\tilde{s}^2)^{n+1}}+\right.\\ &\quad \left.\frac{1}{2\pi}\sin(\pi x')-\frac{1}{\pi}\cos^2(\frac{\pi}{2}x')\right]\frac{\Delta\tau}{\Delta x'}\end{aligned} \tag{25}$$

Introducing the variable $B = \tilde{s}^2$, the finite-difference form of Eq. (17) is

$$\left(\frac{dB}{d\tau}\right)^n = \frac{2S_t}{\pi}\left(\frac{\theta_s(n,I_s-1)-4\theta_s(n,I_s)}{2\Delta x'} - b\frac{4\theta_\ell(n,1)-\theta_\ell(n,2)}{2\Delta x'}\right) \tag{26}$$

and B is obtained from the above equation by the improved Euler method

$$B^{n+1} = B^n + \frac{\Delta\tau}{2}\left[\left(\frac{dB}{d\tau}\right)^n + \left(\frac{dB}{d\tau}\right)^{n+1}\right]. \tag{27}$$

The iteration procedure to get the solution at $\tau^{n+1} = \tau^n + \Delta\tau$ is established by introducing an iteration index p and proceeds as follows:

1. Choose a sufficiently small value τ_0. Obtain the temperature distribution and solid phase thickness at τ_0 from the instantaneous-similarity method [17]. Use this solution as the initial field to start the numerical calculation.

2. Calculate $\left(\frac{dB}{d\tau}\right)_p^{n+1} = \left(\frac{dB}{d\tau}\right)^n$ from Eq. (26).

3. Calculate B_p^{n+1} by the Euler method

$$B_p^{n+1} = B^n + \Delta\tau \left(\frac{dB}{d\tau}\right)^n \tag{28}$$

4. Use the value of B_p^{n+1} and $\left(\frac{dB}{d\tau}\right)_p^{n+1}$ to calculate c_1, c_2, d_1, and d_2 from Eqs. (21), (22), (24) and (25). Then solve Eqs. (20) and (23) to obtain θ_s and θ_ℓ by the TDMA method [19].

5. Calculate $\left(\frac{dB}{d\tau}\right)_{p+1}^{n+1}$ from Eq. (26), and calculate B_{p+1}^{n+1} from Eq. (27).

6. If

$$\left|\left(\frac{dB}{d\tau}\right)_{p+1}^{n+1} - \left(\frac{dB}{d\tau}\right)_p^{n+1}\right| \leq \epsilon,$$

$$|B_{p+1}^{n+1} - B_p^{n+1}| \leq \epsilon,$$

$$|\theta_\ell(n+1,i)_{p+1} - \theta_\ell(n+1,i)_p| \leq \epsilon,$$

and,

$$|\theta_s(n+1,i)_{p+1} - \theta_s(n+1,i)_p| \leq \epsilon,$$

the solution at $\tau^{n+1} = \tau^n + \Delta\tau$ is reached. Otherwise, let $\left(\frac{dB}{d\tau}\right)_p^{n+1} = \left(\frac{dB}{d\tau}\right)_{p+1}^{n+1}$, $B_p^{n+1} = B_{p+1}^{n+1}$, and go back to step (4).

3. Numerical Considerations

The transformed system of equations (15)-(16) has a singularity at $\tau = 0$ ($\tilde{s} = 0$). Due to this fact, the numerical solution cannot be started at $\tau = 0$ but instead must be initiated at some sufficiently-small time $\tau = \tau_0$. Rangel and Bian [17] showed that the instantaneous-similarity solution yields the correct limiting form of the solution for $\tau \to 0$. In order to determine an appropriate value for τ_0, we consider the case of $S_t = \theta_i = a = b = 1$, and carry out the numerical solution for starting times $\tau_0 = 1, 0.1, 0.01$, and 0.005. In all cases, the solution obtained with the instantaneous-similarity method is used as the initial

condition. Figure 1a shows the temporal growth of the solidification front as obtained from the finite-difference solution started at different times in the manner just described. The corresponding temperature distributions are shown in Fig. 1b. Figure 1a shows that there is excellent agreement between the solutions started at $\tau_0 = 0.01$ and $\tau_0 = 0.005$, indicating that the former is an appropriate starting point (note that the two curves corresponding to these two cases are indistinguishable from each other in Fig. 1a). Even the solution started at $\tau_0 = 0.1$ yields satisfactory results. These conclusions are confirmed by the results shown in Fig. 1b for the temperature distribution, which also indicate excellent agreement between the cases started at $\tau_0 = 0.01$ and $\tau_0 = 0.005$.

It should be noted that the instantaneous-similarity solution also yields the correct solution in the limit of $\tau \to \infty$ since it corresponds to the quasi-steady solution in that limit [17]. The benefit of the numerical solution is that it permits one to obtain an accurate solution at intermediate times.

All the numerical results are obtained by setting the number of grid points $I_s = 50$ for the solid phase and $I_\ell = 50$ for the liquid phase. Setting values of I_s or I_ℓ to 20 or 100 show no significant difference in the evolution of the temperature distribution or the solid phase thickness. The time step used by the finite-difference solution for the case with $\theta_i = a = b = S_t = 1$ is $\Delta\tau = 0.001$ for $0.01 \leq \tau \leq 0.1$, and $\Delta\tau = 0.005$ for $0.1 \leq \tau \leq 100$. For cases with smaller θ_i, a, b and S_t, the time step can be larger than that. However, for the cases with higher Stefan number, the time step must be reduced to retain the same accuracy, e.g. for the case with $S_t = 10, a = b = \theta_i = 1$, $\Delta\tau$ is set to be 0.00002 for $0.01 \leq \tau \leq 0.1$.

Figure 2 shows a comparison of the solid-front growth obtained with the three different methods. The quasi-steady method and the instantaneous-similarity method were used in [17]. The other is the finite-difference method used here. The finite-difference solutions use both the instantaneous-similarity and the quasi-steady solution as the initial fields. It can be observed that the quasi-steady method overpredicts the solidification rate while the instantaneous-similarity method underpredicts it. It can also be observed that the three solutions approach the same upper limit as time becomes very large. In addition, the finite-difference solution starting from the quasi-steady initial field goes rapidly to the finite-difference solution which uses the instantaneous-similarity solution as the initial field. This demonstrates that the finite-difference solution converges to the correct long-time behavior even if it is started with an inaccurate initial condition, such as the one obtained from the quasi-steady solution.

Figure 3 shows a comparison of the temperature distributions obtained with the same three methods mentioned above. It can be observed that during the initial stages of solidification ($\tau = 0.1$), the numerical solution is much closer to the instantaneous-similarity solution than to the quasi-steady solution, as expected. At $\tau = 1$, the numerical solution lies between the solution obtained with the two analytical methods. Again expectedly, as time becomes very large ($\tau = 100$), the three solutions converge to the same result, with the instantaneous-similarity method behaving better than the quasi-steady solution.

In order to determine the appropriate starting value τ_0 for cases other than the base case discussed above, a similar comparison should be carried out. Because of the known behavior of the solution for smaller values of the Stefan number [17] and in particular, because it has been established that the instantaneous-similarity solution becomes increasingly more accurate as $S_t \to 0$, it is satisfactory to employ a value of $\tau_0 = 0.01$ for any case with $S_t \leq 1$. On the other hand, for the cases with larger Stefan number, we need to evaluate what the appropriate τ_0 is. Such an evaluation is illustrated in Fig. 4, which indicates that $\tau_0 = 0.01$ is again an appropriate choice since the results for $\tau_0 = 0.01$ and $\tau_0 = 0.005$ are in excellent agreement. In the following parametric study, all the finite-difference solutions are initiated at $\tau_0 = 0.01$.

4. Parametric Study

This section contains solidification results obtained with the finite-difference method to demonstrate the effect of the Stefan number and the dimensionless ratios θ_i, a, and b. As a reference, approximate values of θ_i, a, b, and S_t for some selected metals are given in Table. 1. In constructing this table, we have chosen the initial liquid temperature to be $T_i = T_m + 100K$ and the substrate temperature to be $T_0 = 300K$. The solid properties are evaluated at $(T_0 + T_m)/2$ while the liquid properties are evaluated at $(T_m + T_i)/2$.

Returning now to the general results, Fig. 5 shows the temperature distribution along the nondimensional x coordinate, $\tilde{x} = x\sqrt{\frac{A}{\alpha_s}} = \eta\sqrt{\tau}$ during the early ($\tau = 0.1$) and late ($\tau = 100$) stages of solidification for cases with different Stefan number. It can be observed that variations in Stefan number bring about changes in the temperature distribution and the interface location in the early stages of solidification when a larger Stefan number results in a more rapidly-growing solid front. At very large time, however, the temperature distribution becomes independent of Stefan number. This long term behavior was demonstrated analytically in [17].

Figure 6 shows the temperature distribution during the early ($\tau = 0.1$) and late ($\tau = 100$) stages of solidification for cases with different values of θ_i, a and b. It can be seen that during the early stages of solidification and at the same position in the liquid phase, the liquid temperature is lower for higher a and b. Realize that a value of a larger than one would typically be associated with a value of b also larger than one. In the early stages of solidification, higher a and b means that heat transfer is more efficient in the liquid phase, and therefore, the liquid temperature drops to a lower value as compared to a case with lower a and b. However, during the late stages of solidification, the temperature distribution and the solid front location approach their asymptotic limits. For a fixed position in the liquid phase or solid phase, the temperature θ_ℓ or θ_s is lower for the cases with lower a, b. Thus, it can be concluded that variations in the parameters a and b affect both the initial and the long time behavior of the solution.

Figure 7 shows the variation of the dimensionless thickness $\tilde{s}$ with τ for different values of the Stefan number for the case of θ_i=1, a=1, b=1. It can be seen that $\tilde{s}$ increases with τ, and that there exists an upper limit of $\tilde{s}$ as τ approaches infinity. It can also be observed that this limit is independent of the Stefan number and that $\tilde{s}$ increases faster for larger S_t. Higher Stefan number is indicative of a larger transfer number or an increase in the energy transfer rate as compared with latent-heat release rate, resulting in a faster solidification rate.

The effect of θ_i, a, and b on the solid front growth rate is shown in Fig. 8 for the same Stefan number. The dimensionless thickness $\tilde{s}$ increases faster for smaller a, b and θ_i. Smaller a, b or θ_i translates into less heat from the liquid to the solid phase through the interface, so that solidification occurs more rapidly.

Figure 9 shows the growth rate of the solid-liquid interface location and the time variation of the heat fluxes at the interface on both the liquid and solid sides for $S_t = 0.1,\ 1$, and 10. The existence of a finite asymptotic limit for the solidification front in the stagnation-flow problem may be understood with the aid of this figure. Realize that the thermal field in the liquid phase reaches a truly quasi steady behavior after a finite time. This implies that the heat flux at the interface on the liquid side decreases not to zero but to a finite value in the limit of $t \to \infty$. This is not the case in the classical Stefan solidification problem where the heat flux at the interface on the liquid side continues to decrease as $t^{-1/2}$ as $t \to \infty$. Moreover, the behavior of the heat flux at the interface on the solid side is similar for both the classical and the stagnation-flow solidification problems. In the classical problem, the solid thickness s increases as $t^{1/2}$ and thus the solid heat flux

decreases as $t^{-1/2}$, the same rate of decrease of the liquid heat flux. Since energy arriving at the interface by conduction from the liquid must ultimately be conducted through the solid into the substrate, the solid heat flux must be at least as large as the liquid heat flux. It is actually larger since it must also carry the latent heat of solidification released at the interface. In the stagnation-flow solidification problem, the solid front can only rise to a height which results in a solid heat flux equal to the liquid heat flux. At that point, no further solidification is possible.

5. Conclusions

The stagnation-flow solidification problem has been solved numerically employing a finite-difference method. The Crank-Nicolson method is applied to obtain the finite-difference form of the liquid and solid phase energy equations, and the resulting difference equations are solved by the TDMA method. The location of the liquid-solid interface is tracked by solving the interface energy balance equation coupled with the solid and liquid phase energy equations. To avoid the singularity of the transformed system of equations at the starting time ($\tau = 0$), the instantaneous similarity solution [17] at a sufficiently-small time is used to initiate the finite-difference solution. The effect of the selected initial time τ_0 on the accuracy of the finite-difference solution is evaluated. Comparisons of the temperature distributions and solid phase thicknesses obtained with the three methods show that in the initial stages of solidification ($\tau = 0.1$), the finite-difference method and the instantaneous-similarity method yield equivalent results, while the quasi-steady prediction of the solid phase thickness is higher. At intermediate times ($\tau = 1$), the finite-difference solution, which can be considered exact, lies between the instantaneous similarity solution and the quasi-steady solution. At very large time ($\tau = 100$), the three solutions converge and the results show that the temperature distribution and the interface location approach a quasi-steady behavior as time becomes very large. The results confirm the existence of an important difference in the solidification behavior between the classical Stefan solidification problem and the stagnation-flow solidification problem as the latter results in a finite solid thickness as $\tau \rightarrow \infty$.

Acknowledgement

This work has been supported by a grant from the National Science Foundation (CTS-9224856).

References

[1] S. H. Cho and J. E. Sunderland, Heat-Conduction Problems with Melting or Freezing, *J. Heat Transfer*, vol. 91c, pp. 421-426, 1969.

[2] J. Madejski, Solidification of Droplets on a Cold Surface, *Int. J. Heat Mass Transfer*, vol. 19, pp. 1009-1013, 1976.

[3] J. Madejski, Droplets on impact with a solid Surface, *Int. J. Heat Mass Transfer*, vol. 7, pp. 1095-1098, 1983.

[4] K. Brattkus and S. H. Davis, Flow induced Morphological Instabilities: Stagnation-Point Flows, *J. Crystal Growth*, Vol. 89, pp.423-427, 1988.

[5] A. A. Rostami, R. Greif and R. E. Russo, Modified Enthalpy Method Applied to Rapid Melting and Solidification, *Int. J. Heat Mass Transfer*, vol. 35, pp. 2161-2172, 1992.

[6] L. E. Goodrich, Efficient Numerical Technique for One Dimensional Thermal Problems with Phase Change, *Int. J. Heat Mass Transfer*, vol. 21, pp. 615-621, 1978.

[7] W. Shyy, H. S. Udaykumar and S. J. Liang, An Interface Tracking Method Applied to Morphological Evolution during Phase Change, *Int. J. Heat Mass Transfer*, vol. 36, pp. 1833-1844, 1993.

[8] A. Y. Belekii and S. N. Zolotarev, Theoretical Analysis of Fluid Dynamics and Heat Transfer in the Single Roller Rapid Solidification Method, *Int. J. Rapid Solidification*, vol. 6, pp. 41-54, 1991.

[9] T. Bennett and D. Poulikakos, Splat-Quench Solidification: Estimating the Maximum Spreading of a Droplet Impacting a Solid Surface, *J. Material Science*, vol. 28, pp. 963-970, 1993.

[10] M. Lacroix and V. R. Voller, Finite Difference Solutions of Solidification Phase Change Problems: Transformed versus Fixed Grids, *Numerical Heat Transfer, Part B*, vol. 17, pp. 25-41, 1990.

[11] T. Watanabe, I. Kuribayashi, T. Honda and A. Kanzawa, Deformation and Solidification of a Droplet on a Cold Substrate, *Chemical Engr. Sc.*, Vol. 47, pp. 3059-3065, 1992.

[12] H. Liu, E. J. Lavernia and R. H. Rangel, Numerical Simulation of Substrate Impact and Freezing of Droplets in Plasma Spray Processes, *J. Phys. D: Appl. Phys.*, vol. 26, pp. 1900-1908, 1993.

[13] H. M. Weber, *Die partiellen Differential-Gleichungen der mathematischen Physik nach Riemann's Vorlesungen*, 2nd ed., p. 121, F. Vieweg und Sohn., Braunschweig, 1912.

[14] H. S. Carslaw and J. C. Jaeger, *Conduction of Heat in Solids* , 2nd ed., p. 283, Clarendon Press, London, 1959.

[15] M. N. Ozisik, *Heat Conduction* , 1st ed., p. 439, John Wiley & Sons, New York, 1980.

[16] J. Crank, *Free and Moving Boundary Problems*, 1st ed., pp. 153-252, Clarendon Press, Oxford, UK, 1984.

[17] R. H. Rangel and X. Bian, The Stagnation-flow Stefan Solidification Problem, submitted to *Int. J. Heat Mass Transfer*, 1994.

[18] A. Campo and J.-C. Auguste, Axial conduction in laminar pipe flows with nonlinear wall heat fluxes, *Int. J. Heat Mass Transfer*, vol. 21, pp. 1597-1607, 1978.

[19] S. V. Patankar, *Numerical Heat Transfer and Fluid Flow* , 1st ed., pp. 52-54, McGraw Hill, New York, 1980.

.

Substance	T_m (k)	θ_i	ρ_ℓ/ρ_s	$a = \alpha_\ell/\alpha_s$	$b = k_\ell/k_s$	S_t
Al	933	0.16	0.88	0.43	0.40	1.67
Cu	1356	0.10	0.89	0.44	0.45	2.26
Ni	1727	0.07	0.89	0.77	0.83	2.68
Ti	1958	0.06	0.91	1.01	0.93	2.76
W	3650	0.03	0.91	0.56	0.70	3.05

Table 1. Some practical values of a, b, S_t

Figure Captions

Fig. 1. Effect of the starting time on the finite difference solution. (a) Solidification front vs. time; (b) Temperature distribution.

Fig. 2. Comparison of the solid-front evolution with time obtained with different methods.

Fig. 3. Comparison of the temperature distributions obtained with three different methods.

Fig. 4. Finite-difference temperature distributions obtained with the instantaneous similarity solution as the initial field.

Fig. 5. Comparison of the temperature distributions at early and late stages of solidification: effect of Stefan number.

Fig. 6. Comparison of the temperature distributions at early and late stages of solidification: effect of θ_i, a, and b.

Fig. 7. Increase of the solid phase thickness with time: effect of Stefan number.

Fig. 8. Increase of the solid phase thickness with time: effect of θ_i, a, and b.

Fig. 9. The time variation of the solid and liquid heat fluxes at the interface and the solid-liquid interface growth rate.

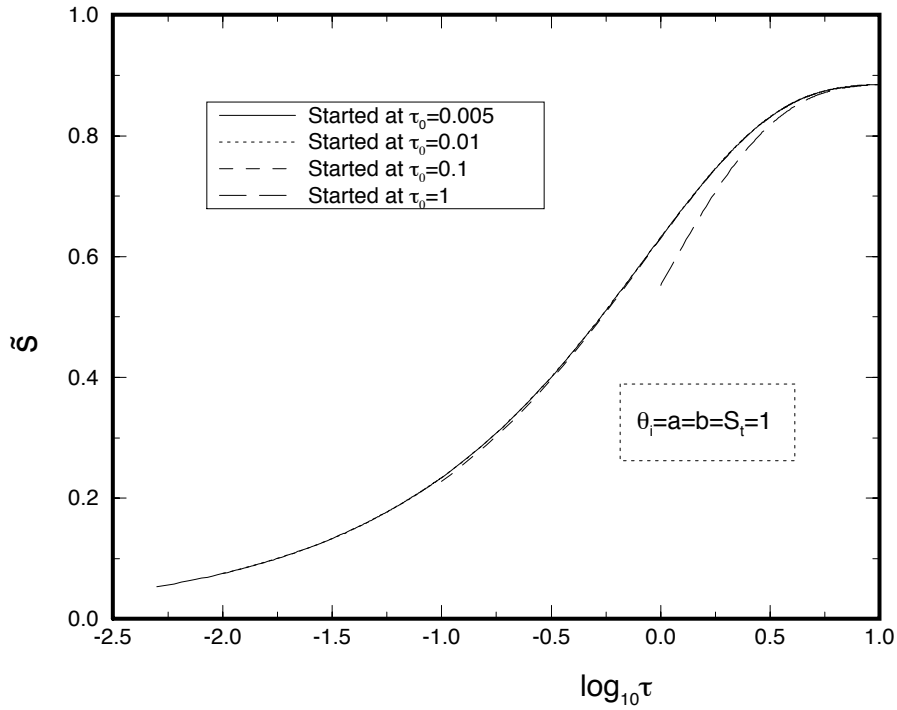

(a)

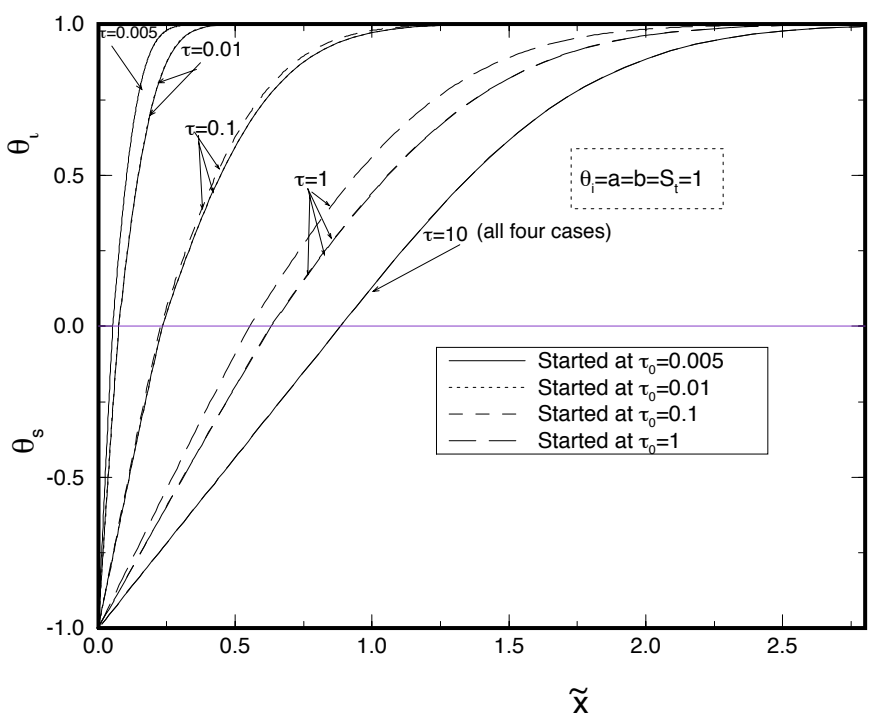

(b)

Fig. 1. Rangel and Bian

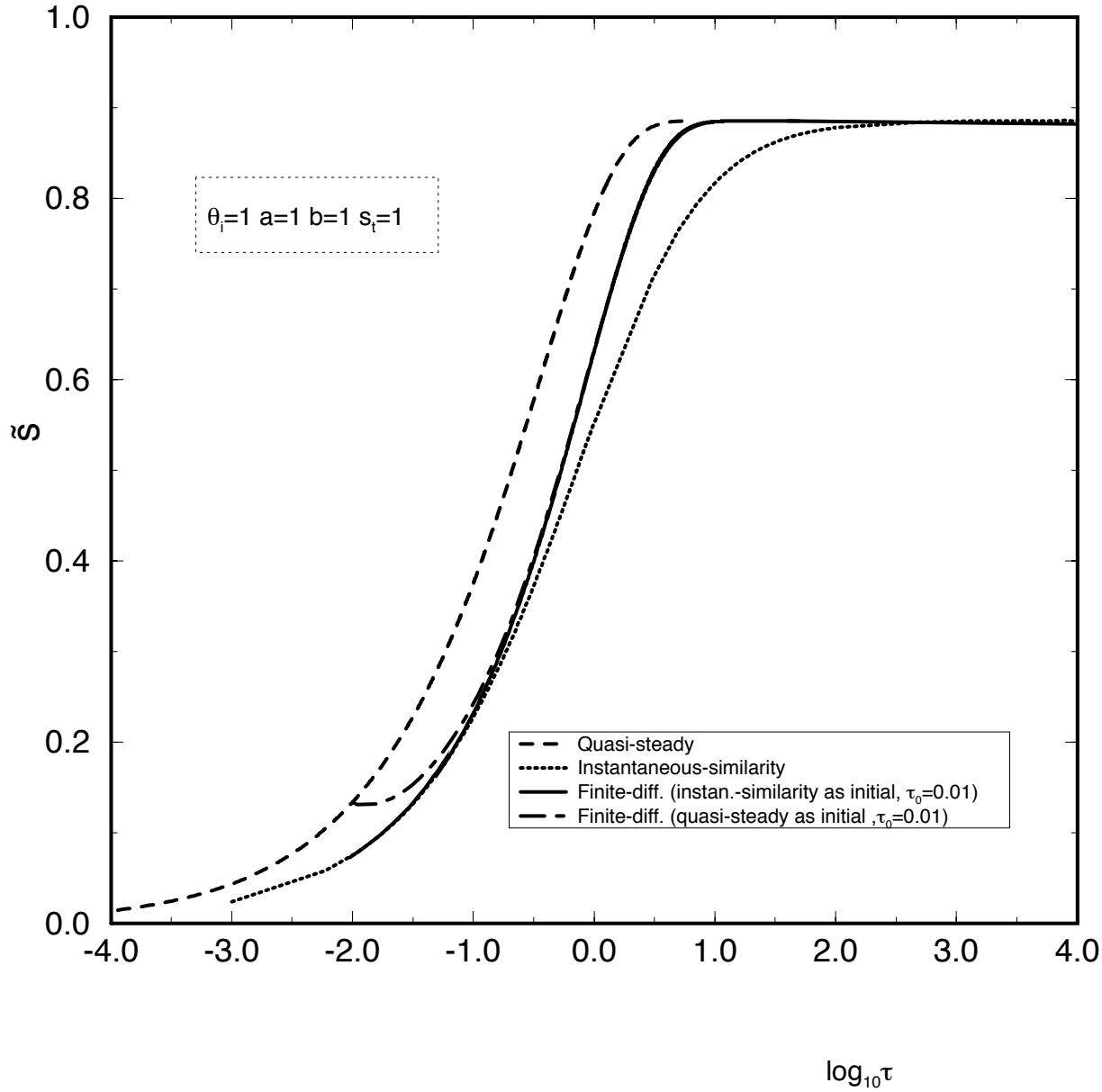

Fig. 2. Rangel and Bian

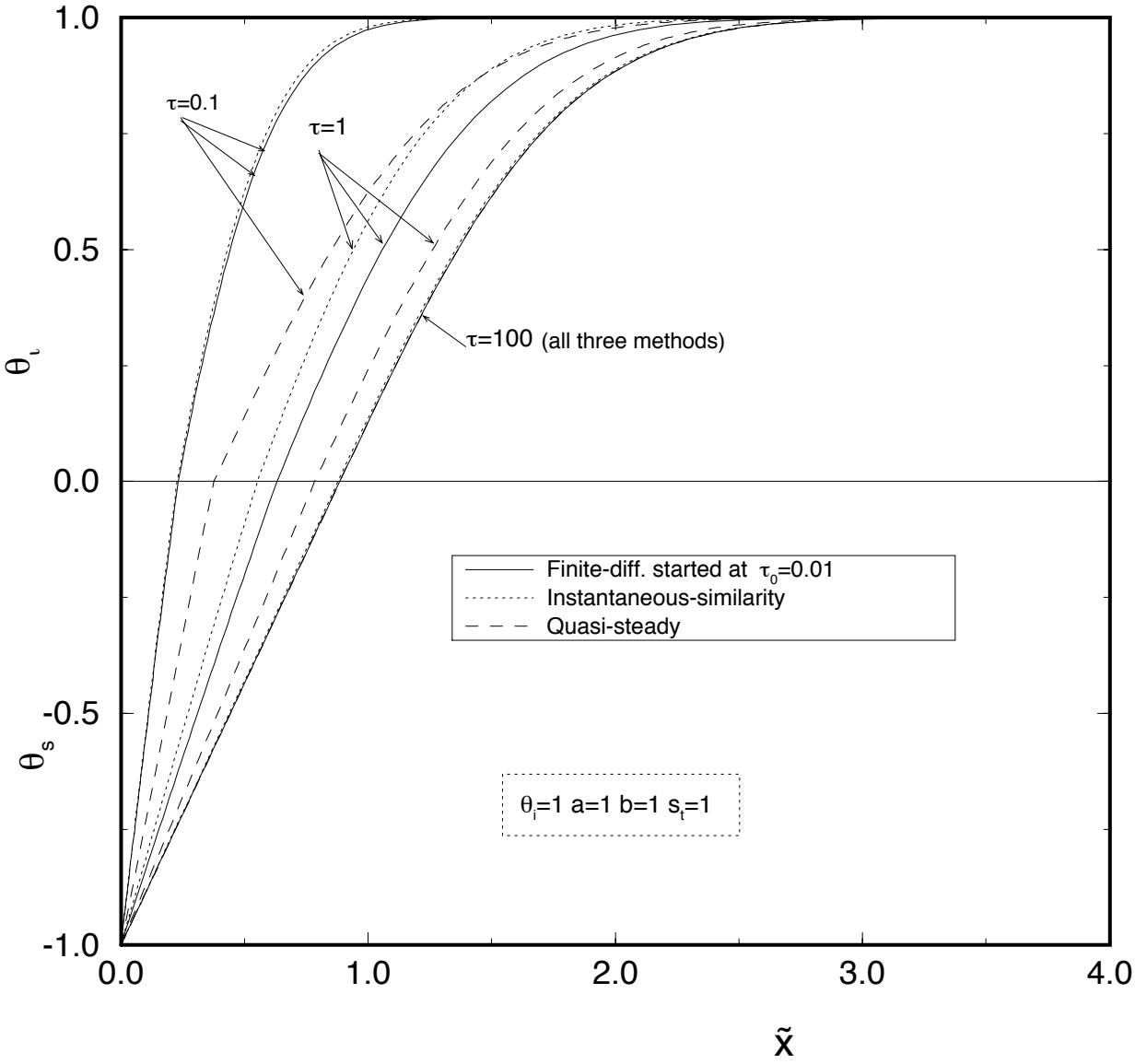

Fig. 3. Rangel and Bian

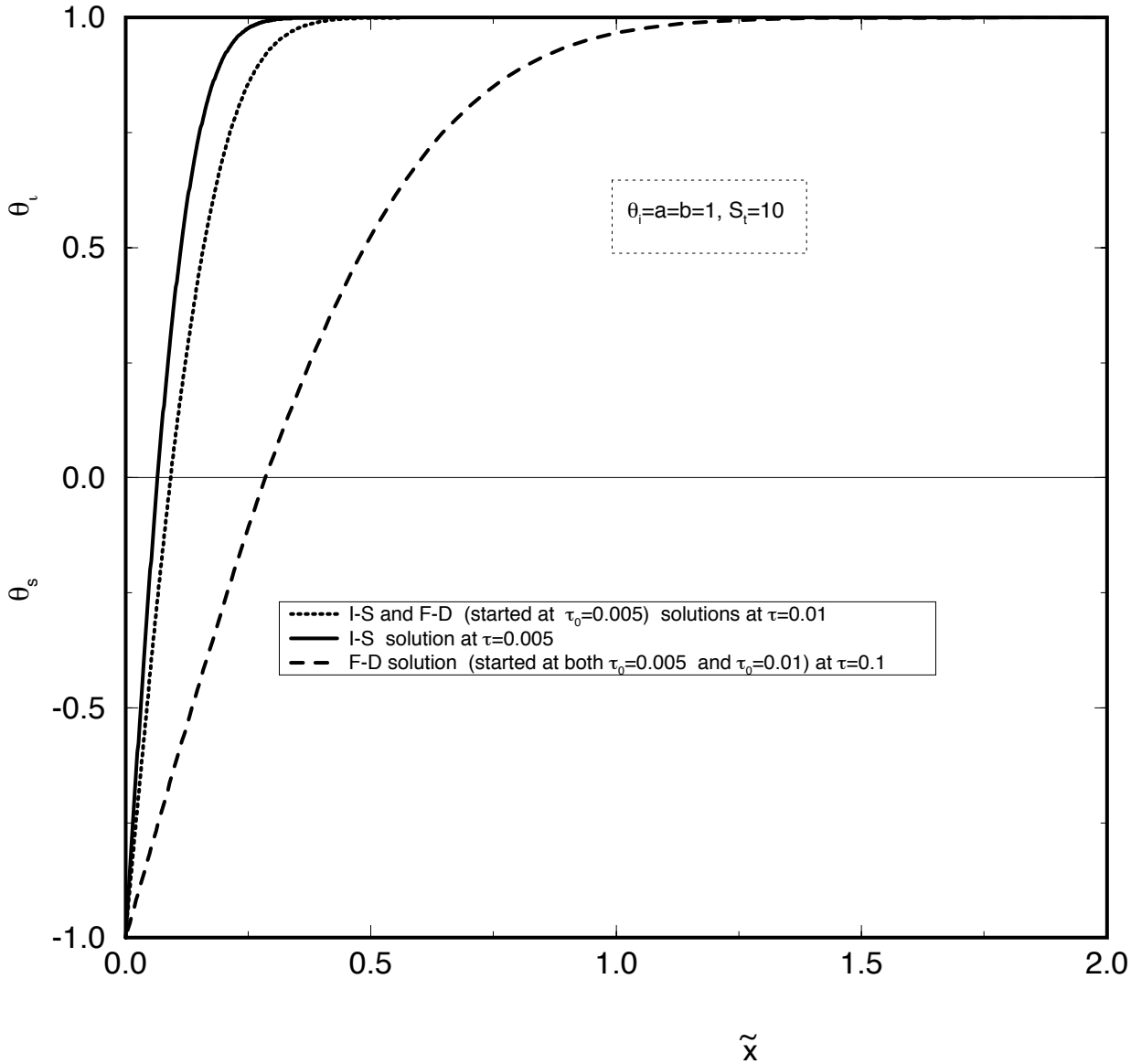

Fig. 4. Rangel and Bian

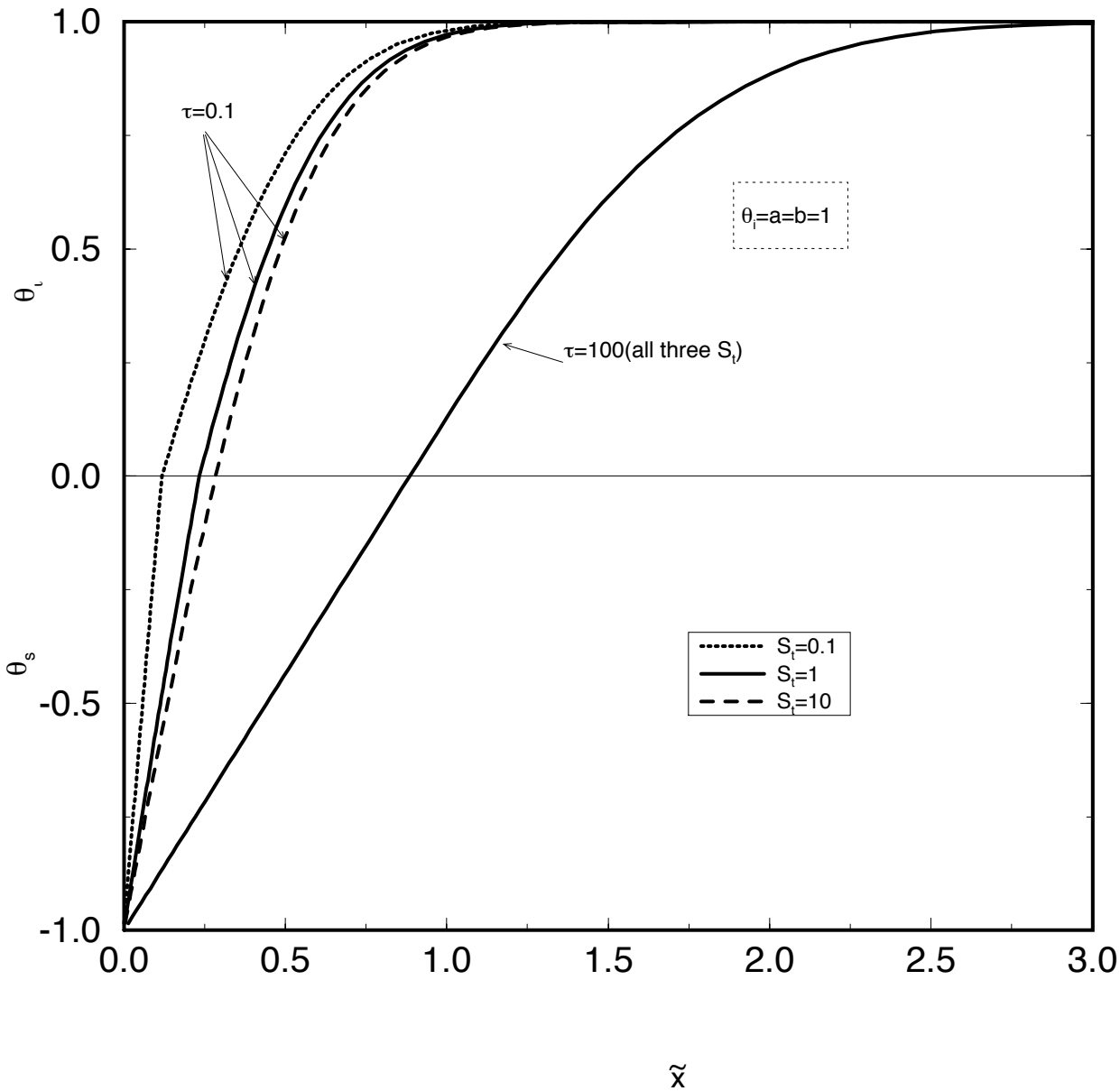

Fig. 5. Rangel and Bian

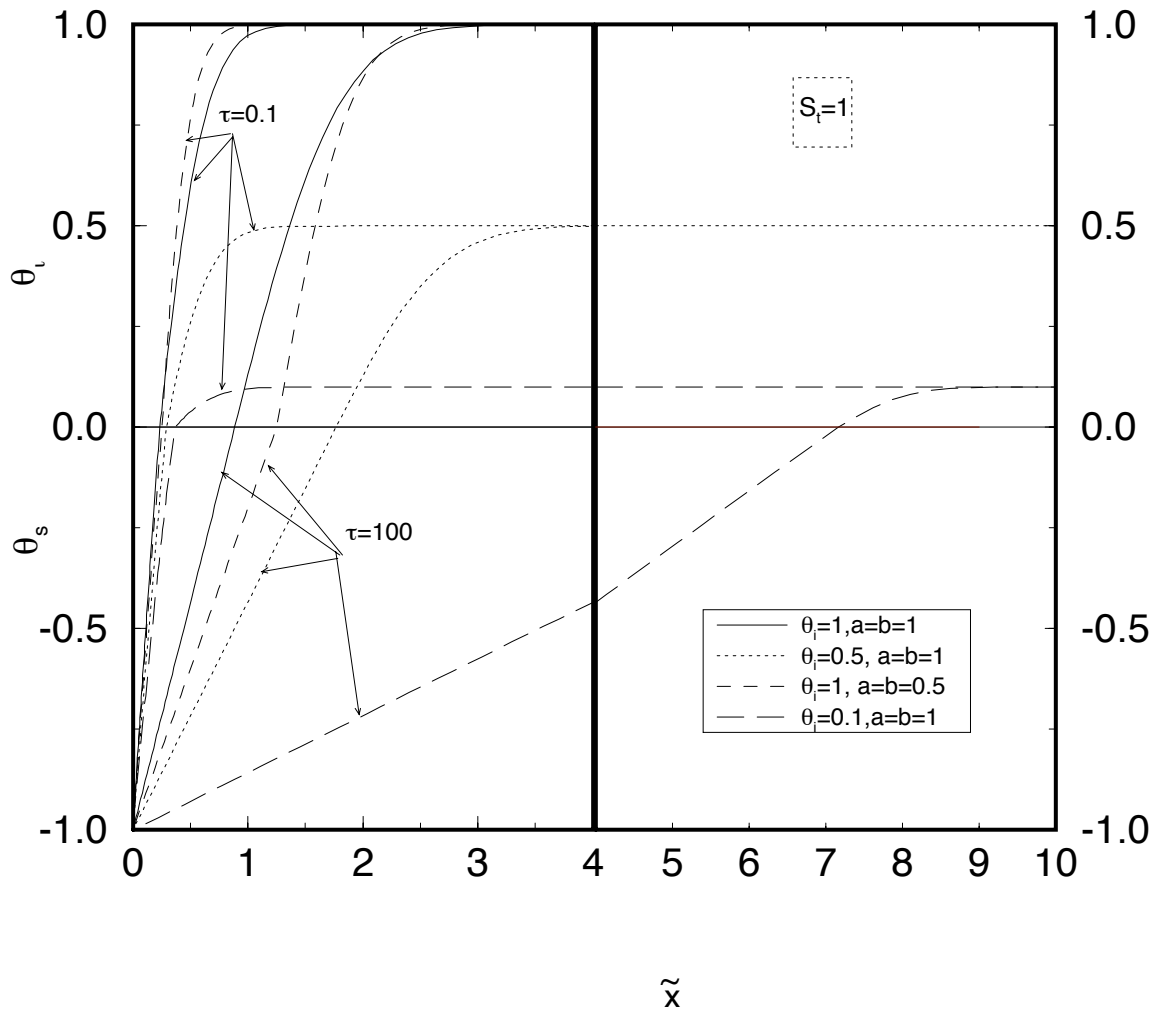

Fig. 6. Rangel and Bian

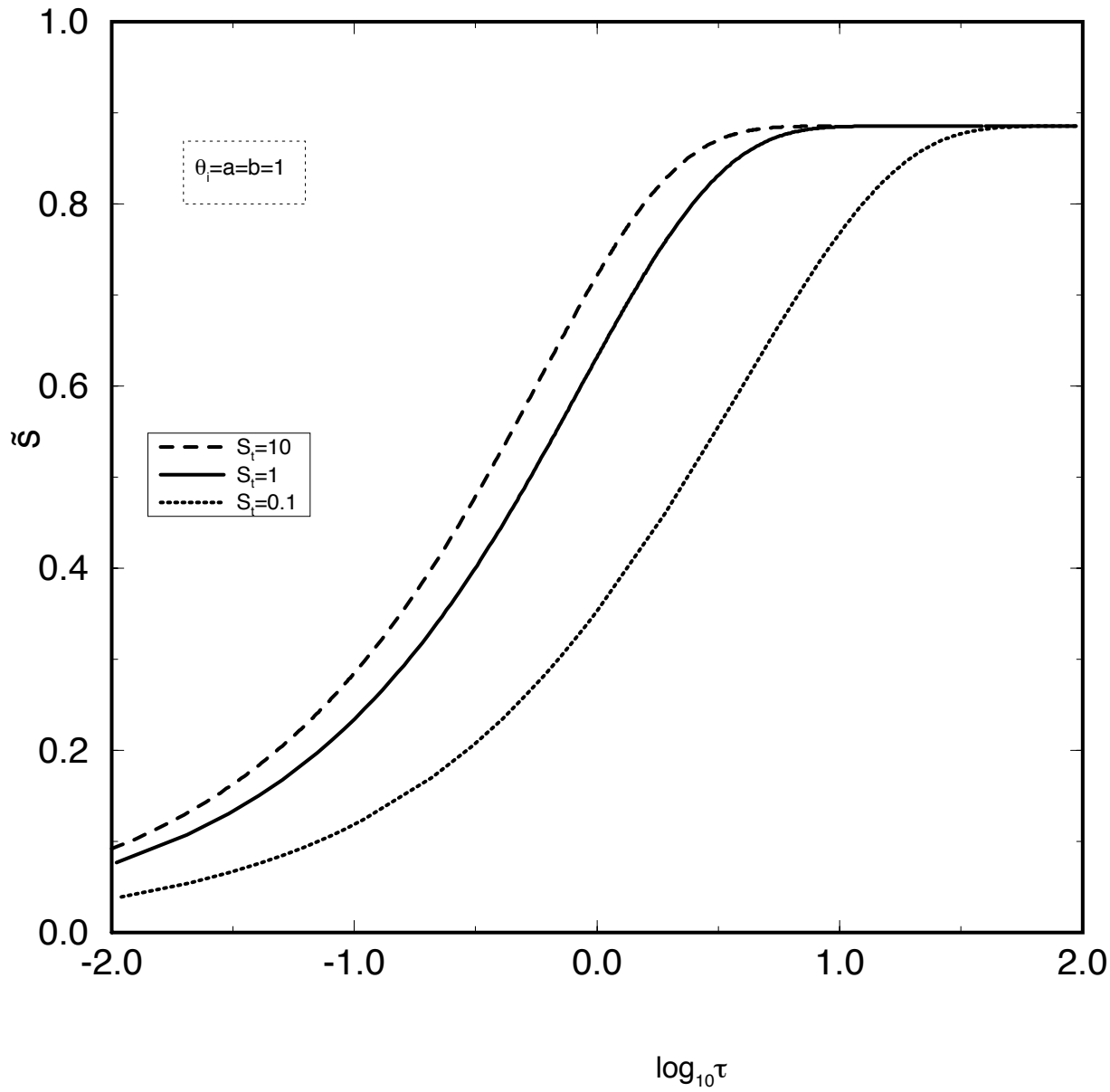

Fig. 7. Rangel and Bian

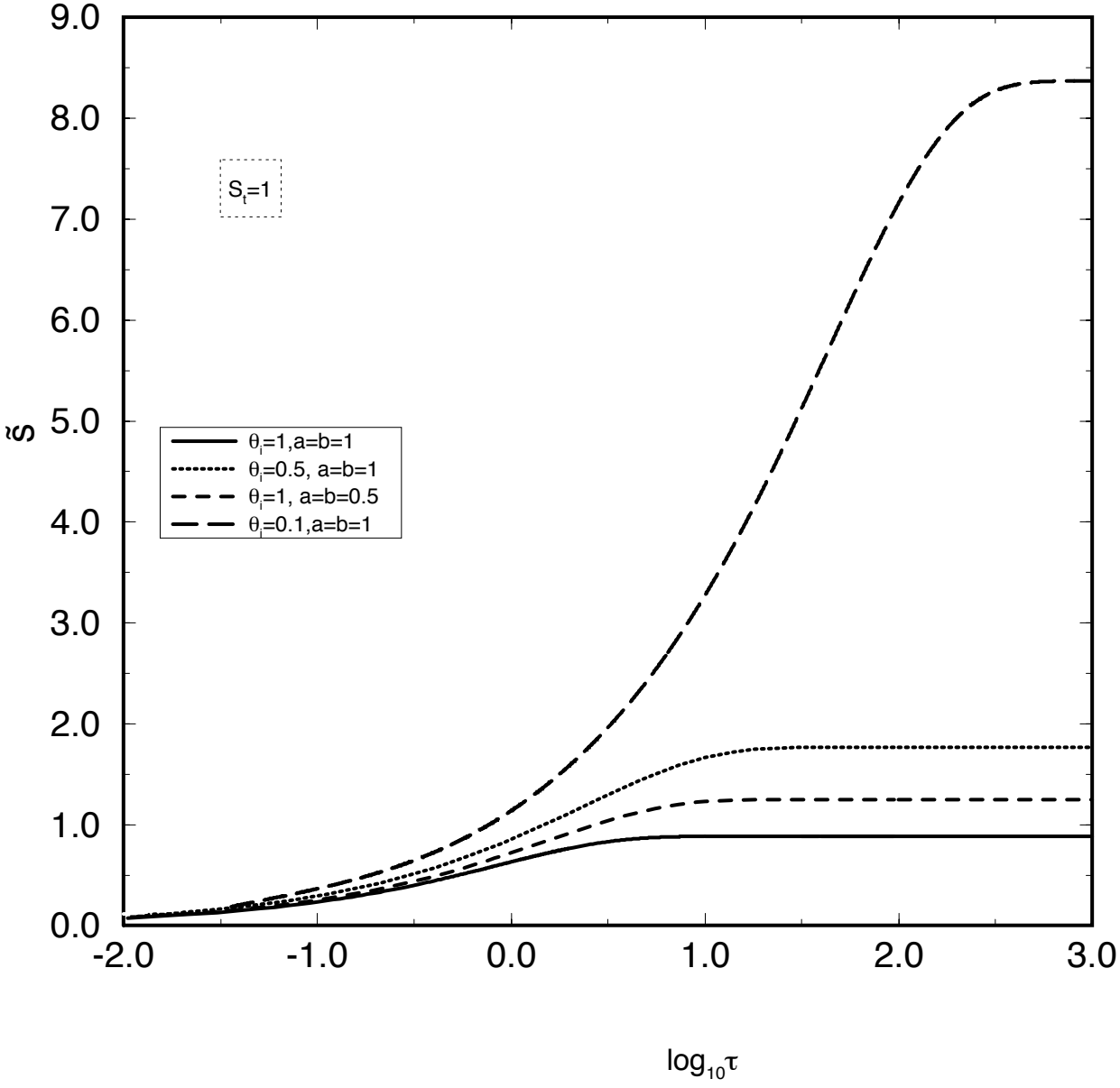

Fig. 8. Rangel and Bian

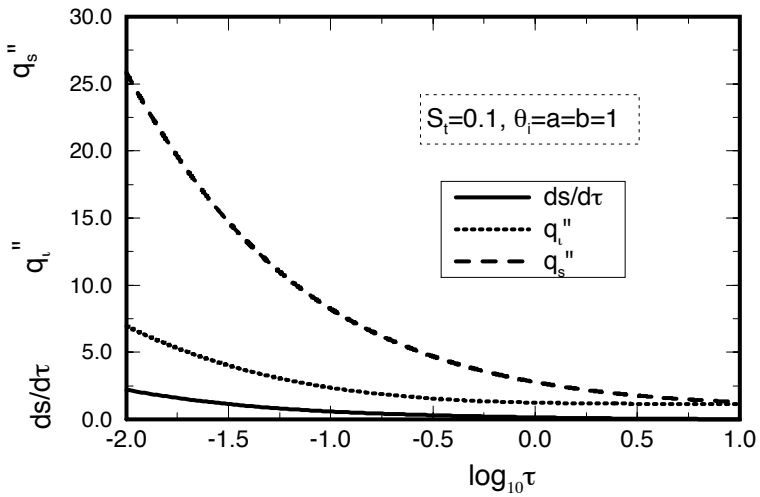

(a)

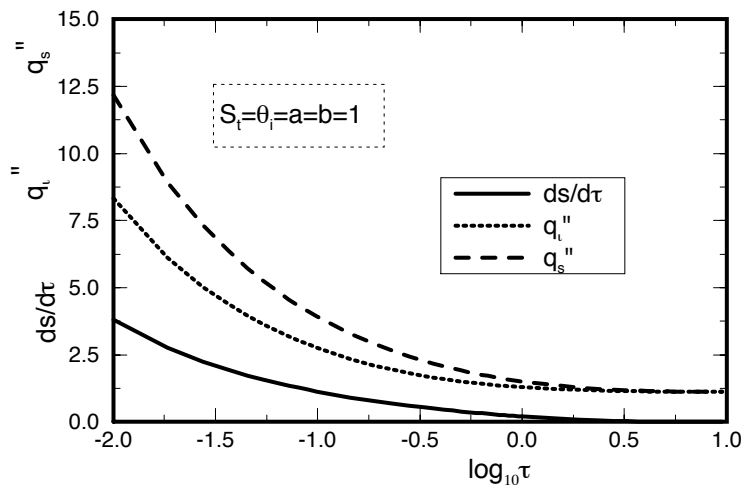

(b)

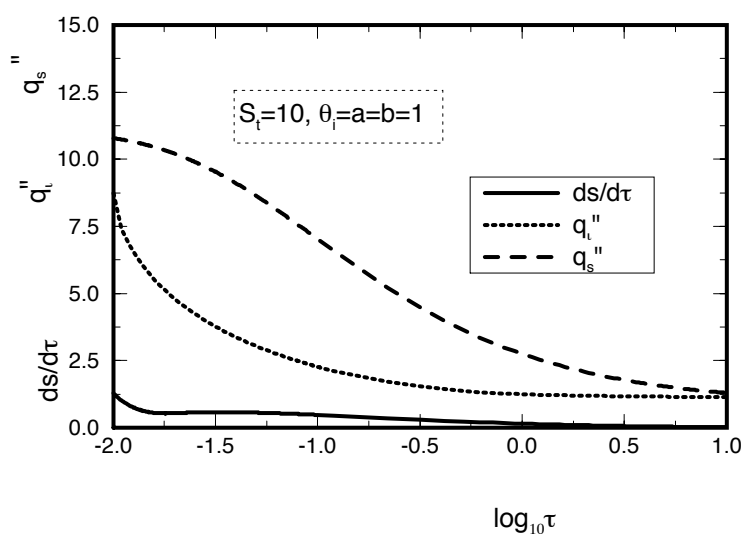

(c)

Fig. 9. Rangel and Bian